Mefloquine targets the *Plasmodium falciparum* 80S ribosome to inhibit protein synthesis

Wilson Wong[1#], Xiao-Chen Bai[3#], Brad E. Sleebs[1#], Tony Triglia[1#], Alan Brown[3], Jennifer K. Thompson[1], Katherine E. Jackson[4], Eric Hanssen[4], Danushka S. Marapana[1], Israel S. Fernandez[3], Stuart A. Ralph[4], Alan F. Cowman[1,2], Sjors H.W. Scheres [3]* and Jake Baum[1,2,5]*

[1] Walter and Eliza Hall Institute of Medical Research, Parkville, Victoria, 3052, Australia.

[2] Department of Medical Biology, University of Melbourne, Parkville, Victoria, 3010, Australia.

[3] MRC Laboratory of Molecular Biology, Cambridge Biomedical Campus, Cambridge CB2 0QH, UK.

[4] Bio21 Molecular Science and Biotechnology Institute, University of Melbourne, Parkville, Victoria 3010, Australia.

[5] Department of Life Sciences, Imperial College London, South Kensington, London, SW7 2AZ, UK.

[#]These authors contributed equally to this work.

*To whom correspondence should be addressed; jake.baum@imperial.ac.uk or scheres@mrc-lmb.cam.ac.uk

Malaria control is heavily dependent on chemotherapeutic agents for disease prevention and drug treatment. Defining the mechanism of action for licensed drugs, for which no target is characterized, is critical to the development of their second-generation derivatives to improve drug potency towards inhibition of their molecular targets. Mefloquine is a widely used antimalarial without a known mode of action. Here, we demonstrate that mefloquine is a protein synthesis inhibitor. We solved a 3.2 Å electron cryo-microscopy structure of the *Plasmodium falciparum* 80S-ribosome with the (+)-mefloquine enantiomer bound to the ribosome GTPase-associated center. Mutagenesis of mefloquine-binding residues generates parasites with increased resistance, confirming the parasite-killing mechanism. Furthermore, structure-guided derivatives with an altered piperidine group, predicted to improve binding, show enhanced parasiticidal effect. These data reveal one possible mode of action for mefloquine and demonstrate the vast potential of cryo-EM to guide the development of mefloquine derivatives to inhibit parasite protein synthesis.

Malaria is a major protozoan parasitic disease that inflicts an enormous burden on global human health. In 2015 the disease resulted in an estimated 429,000 deaths with several hundreds of millions of people infected [1]. The causative agents of malaria are a group of protozoan parasites that belong to the genus *Plasmodium,* a member of the ancient apicomplexan phylum of vertebrate pathogens, with *P. falciparum* and *P. vivax* being responsible for the majority of disease mortality and morbidity, respectively [2].

Antimalarial chemotherapies have long been the gold-standard utility for the prevention and treatment of malaria. Over many decades, different classes of antimalarials have been clinically approved and deployed as frontline treatments to combat malaria disease [3]. Despite the long-standing usage of these drugs, their mode of actions in mediating parasite killing are not well defined. Mefloquine (MFQ) has been one of the most effective antimalarials since it was first developed and has been used as a chemoprophylactic drug by visitors staying in malaria endemic areas. Neurological side effects associated with MFQ usage [4], have precluded the drug being used widely as a first choice for

preventative treatment. MFQ has, however, been used in combination with the front line antimalarial drug artemisinin globally to treat malaria, constituting one of the many classes of artemisinin-combination therapies (ACT) pivotal to malaria control. Importantly, in regions that have prevalent pools of artemisinin resistant parasites, recent reports have shown that artemisinin-resistant strains of *P. falciparum* are sensitive to MFQ due to decreasing copy number of Pf*mdr1*, a marker of mefloquine resistance [5]. In an urgent response to stem the spread of ACT resistant parasites beyond the province of western Cambodia, the World Health Organization (WHO) has recommended the re-introduction of artesunate and MFQ combination therapy in those regions to combat multi-drug resistant strains of *P. falciparum* [6]. Conversely, in regions where MFQ resistance is prevalent, dihydroartemisinin-piperaquine treatment is preferentially deployed. Despite the major role of MFQ in malaria prevention and its utility in controlling resistant parasites to other ACTs, the molecular basis for its mode of action is, however, not known. Previous studies have suggested that the molecular target(s) for MFQ likely resides in the parasite cytoplasm since efflux of MFQ from the cytoplasm to the parasite food vacuole by the Pf*mdr1* encoded drug transporter Pgh-1, is the predominant mechanism of MFQ resistance [7-10]. Furthermore, a large-scale screen of antimalarial drugs previously implied that MFQ might be a putative inhibitor of the *P. falciparum* cytoplasmic ribosome [11]. To this end, defining the mode of action of MFQ in the malaria parasite along with high-resolution structural elucidation of the drug bound to its target would enable structure-guided development of mefloquine derivatives to enhance drug inhibition on the molecular target(s).

Here, we demonstrate that MFQ mediates killing of the malaria parasite by inhibition of parasite protein synthesis through direct binding to the cytoplasmic ribosome (Pf80S) of *P. falciparum*. We have solved the cryo-EM structure of the Pf80S ribosome in complex with MFQ at 3.2 Å resolution, revealing the interaction between the (+)-MFQ enantiomer with residues within the GTPase-associated center of the Pf80S ribosome. The mechanism of parasite killing by MFQ via Pf80S is confirmed by genetic interrogation of key binding residues, with transgenic parasites possessing amino acid substitutions predicted to alter MFQ binding showing enhanced resistance to the drug.

Furthermore, using the high-resolution cryo-EM structure as a reference, we designed *de novo* MFQ derivatives with modifications to a critical MFQ piperidine group and demonstrated that these MFQ derivatives have enhanced antimalarial activity correlating with the structure-activity relationship. Collectively, these data establish the Pf80S ribosome as one of the molecular target(s) of MFQ-mediate parasite killing. Our cryo-EM structure of the Pf80S-MFQ complex serves as an important reference for the design of new MFQ-based derivatives, expanding available tools to inhibit parasite protein synthesis.

MFQ inhibits cytosolic protein synthesis in *P. falciparum*

We first determined the half maximum inhibitory concentration (EC_{50}) of MFQ-mediated killing of the 3D7 strain of *P. falciparum,* which showed potent antimalarial activity, with an EC_{50} of 25.3 nM (Table 1). The effect of MFQ on translation activity was then tested using incorporation of radiolabelled S_{35}-methionine and S_{35}-cysteine as reporters for protein synthesis. MFQ inhibited protein synthesis by 55%, while parasites cultured in the presence of a non-translation inhibitory compound chloroquine (CQ) showed no inhibition (Fig. 1a; t-test versus CQ, $p < 0.05$, both 3D7 and W2mef strains). MFQ-mediated translation inhibition was, however, weaker than other, highly toxic cytosolic translation inhibitors such as cycloheximide (CHX) (90%; t-test versus CQ, $p < 0.05$, both 3D7 and W2mef strains) (Fig. 1a). Parasites incubated with doxycycline (DOX), a translation inhibitor that is believed to target only the ribosome of the parasite plastid (apicoplast) organelle[12, 13], showed no effect on cytosolic translation (Fig. 1a). No obvious parasite morphological changes following drug treatment were observed with parasites treated with various antimalarials (CQ, CHX, DOX, EME, MFQ and QUI) showing intact mitochondria and nucleus (Supplementary Fig. 1), indicating the assay conditions did not result in significant non-specific cytotoxicity. Collectively, these results support the hypothesis that MFQ is an inhibitor of cytosolic translation.

Cryo-EM structure of the Pf80S-MFQ complex at 3.2 Å resolution

To demonstrate that MFQ directly acts on the parasite 80S ribosome, we solved the structure of *P. falciparum* cytoplasmic ribosome (Pf80S) in the presence of MFQ racemic mixture by cryo-EM at an overall resolution of 3.2 Å (Fig. 2a-c, Supplementary Data Table 1). A difference map calculated between this reconstruction and Pf80S in its apo-form[14] showed two independent continuous densities with shape and size congruent with MFQ when visualized at a threshold of 5 standard deviations (Supplementary Fig. 3a). The well-resolved densities enabled the accurate placement of two MFQ molecules (Fig. 2a-b, Supplementary Fig. 3). The primary MFQ binding-site (designated based on location and correlation with MFQ tolerance, as described below) was located within the GTPase-associated center (GAC) of the large ribosomal subunit (Pf60S) (Fig. 2c and 2e), comprised from the protein uL13, the sarcin-ricin loop of uL6, ribosomal RNA helices 94-5 and expansion segment (ES) 13, where this site interacted with a (+) enantiomer of the MFQ molecule ((+)-MFQ). This region is critical for translation, coordinating the elongation steps of protein synthesis by binding the translational GTPases, and activating the energy dependent translocation of the tRNA-mRNA complex through the ribosome[15, 16]. A secondary binding site was located at the peripheral surface of the Pf60S subunit (Supplementary Fig. 3b) where this site interacted with a (-) enantiomer of the MFQ molecule. Two residues (Tyr290 and His294) from uL4 form a pocket that accommodates the quinoline ring of MFQ at this secondary site (Supplementary Fig. 3b). In *P. vivax*, however, His294 is substituted by Ser294 in this distal MFQ binding site (Supplementary Fig. 3c). Since *P. vivax* is sensitive to MFQ, divergence in this secondary binding site does not, as such, correlate with the inhibitory activity of MFQ on *P. falciparum* and *P. vivax*. Furthermore, since this region has no known role in translation, we believe it is unlikely that MFQ binding at such a site could impact protein synthesis. Of note, the observation of primary (functional) and secondary (likely physiologically irrelevant) binding sites for the antibiotic tetracycline have similarly been reported previously[17].

The identified primary MFQ binding site lies within a crevice formed by a helix of the ribosomal protein uL13 (residues 45 – 59) and ES13 of 28S rRNA (Fig. 2d and 3a). The non-polar residues Leu15 and Ile42 of uL13 interact with the hydrophobic trifluoromethyl group (CF_3) located on C_8 of the quinoline

ring (Fig. 3a). On the opposite end of the quinoline ring, the 2-CF_3 group forms a hydrophobic interaction with two aromatic residues (Tyr53 and Phe56) of uL13 (Fig. 3a). The quinoline ring is further stabilized through a cation-Pi interaction with a magnesium ion coordinated to the backbone phosphate of base C1442 (Fig. 3a). The hydroxyl group of the linker that bridges the quinoline and piperidine ring forms a hydrogen bond with the phosphate backbone of base G1441 (Fig. 3a). Finally, the secondary amine group of the piperidine ring forms a further hydrogen bond with Glu55 of uL13 (Fig. 3a). The inter-atomic distances between (+)-MFQ and interacting residues are within the range of 2.6 – 3.5 Å (Fig. 3b). The nature of this binding site is consistent with structure-activity studies when MFQ was originally conceived [18]. Thus, all three functional moieties of (+)-MFQ (quinoline, piperidine ring and the hydroxyl linker) are required for binding to the GAC, while a combination of hydrophobic and hydrogen bonds form the basis of the interaction. To our knowledge, this site of the eukaryotic 80S ribosome represents a novel binding site for a translation inhibitor. Although the thiopeptide and orthosomycin classes of antibiotics also target the GAC, they interfere directly with the binding of elongation factors to the ribosome (Supplementary Fig. 4) [19]. However, given that MFQ and thiopeptide/orthosomycin each target the GAC, this suggests that MFQ functions to inhibit parasite protein synthesis by inhibiting the polypeptide elongation step.

MFQ binding residues of protein uL13 of the Pf80S confer functional parasite killing by MFQ

To assess if the primary MFQ binding site in uL13 is the site of action for MFQ-mediated parasite killing, targeted mutagenesis was conducted using CRISPR genome editing technology[20]. Amino acid substitutions (Leu15Ser and Ile42Ser) were introduced into uL13 in 3D7 parasites (Supplementary Fig. 5, Supplementary Data Tables 2-3), while wild type residues (Leu15 and Ile42) were introduced as a positive control. In the control experiment, parasites were obtained within two weeks under drug selection using the dihydrofolate reductase inhibitor, WR99210, however no parasites were recovered in two separate experiments when attempts were made to introduce both Leu15Ser and Ile42Ser. This implies that Ser substitutions of Leu15 and Ile42 in uL13 disrupt the function of GAC of the Pf80S ribosome, leading to parasite death. These data demonstrate the essentiality of the GAC for parasite

viability, suggesting (+)-MFQ binding to this site may contribute to parasite death. Consequently, we introduced single substitutions to the MFQ binding pocket (Ile42Ala, Glu55Ala, Phe56Ala, Leu140Phe) creating four transgenic parasite lines. All four transgenic parasite lines carrying single substitutions were recovered in two weeks under WR99210 drug selection. MFQ sensitivity testing of each were compared to control parasites carrying an integrated wild type uL13 gene to test the significance of the MFQ uL13 binding pocket in parasite killing. Despite numerous attempts to purify pure (+) and (-) enantiomers of MFQ with different methods, purification of the MFQ chiral enantiomers for drug sensitivity testing was not possible for this study. As a result, we performed MFQ sensitivity testing using a racemic mixture. Transgenic parasites carrying each single amino acid substitution were more resistant to MFQ, which gave EC50s 1.4 – 1.7 fold higher (36.6 nM – 43.8 nM) than control parasites transfectant for the wild type allele (EC50 = 26 nM) (Fig. 3c, Table 1, p values < 0.05). These data confirm the primary MFQ binding pocket in PfuL13 of the 80S ribosome contributes to MFQ-mediated parasite killing.

Previous studies have demonstrated that sexual stages of *P. falciparum* are insensitive to MFQ[21, 22]. During this phase, the parasite switches to variant forms of rRNA that together with the ribosomal proteins form an S-type ribosome that is distinct from the A-type ribosomes found in asexual stages[23]. Comparison of the RNA sequence of the MFQ binding pocket between rRNA variants reveals a single base deletion within ES13 of the S-type ribosome (C1440 deletion, A-type numbering) (Fig. 3d). Such a change is expected to disrupt the local conformation of the primary MFQ binding pocket thus potentially explaining the resistance of gametocytes to MFQ. Finally, structural conservation of the new binding pocket was explored to determine if it was predictive of tolerance of other major protozoan parasites to MFQ. Each of the binding elements are strictly conserved between *P. vivax* and *P. falciparum* (Fig. 3e), which is consistent with the MFQ sensitivity of *P. vivax*[24]. *Trypanosoma brucei* is also sensitive to MFQ[25], and most of the MFQ-binding elements are identical except for a conservative Glu55Gln substitution (Fig. 3e) that would preserve the hydrogen bond formed with the NH group on the piperidine ring of MFQ. In contrast, *Toxoplasma gondii,* which is insensitive to MFQ[26],

has a non-conservative Glu55Arg substitution that would be predicted to sterically hinder binding of the piperidine ring moiety (Fig. 3e).

Cryo-EM structure based design of MFQ derivatives with enhanced antimalarial activity

Our high-resolution cryo-EM structure of the Pf80S-MFQ complex serves as a reference-guide to develop MFQ derivatives with improved potency towards inhibition of the Pf80S ribosome. Comparative structural analysis with the human cytosolic ribosome[27] revealed two non-conservative substitutions in uL13 found within the MFQ binding pocket (Supplementary Fig. 6a). The first substituted residue (Glu55Ala; *Pf:* human) would eliminate the hydrogen bond between the NH group of the piperidine ring and uL13 (Fig. 3a and Supplementary Fig. 6a). As already shown, when a Glu55Ala substitution is performed in *P. falciparum*, it leads to lower MFQ binding and thus a higher EC_{50} as expected (Table 1). The second substituted residue (Leu59Lys) would sterically inhibit the binding of MFQ by clashing with C_4 of the piperidine ring (Fig. 1b, 3a and Supplementary Fig. 6). This suggested that this site could be exploited to enhance drug affinity towards the *P. falciparum* 80S ribosome. Furthermore, substantial structural differences in the MFQ binding pocket of the human mitochondrial ribosome[28] indicates that MFQ should not be able to inhibit human mitochondrial protein synthesis (Supplementary Fig. 6b).

As a proof of concept towards this goal, we designed derivatives of MFQ possessing hydrophobic groups that would extend into the parasite-specific Leu59 region of the binding pocket (Fig. 4a-d, Supplementary Data Table 4), while maintaining hydrogen bond interactions with Glu55 and the G1441 nucleotide. Synthesis of these MFQ derivatives (following previously described methods [29, 30]) and evaluation against *P. falciparum* parasites in culture demonstrated subset of these derivatives (MFQ_D3-5) showed 1.9 – 2.4 fold enhancement in potency towards parasite killing (Table 1: $P < 0.05$). Thus, changes in parasite inhibitory potency of MFQ derivatives was found to be entirely consistent with interaction of MFQ to the PfuL13 binding pocket.

DISCUSSION

198 Understanding the mode of actions of clinically used antimalarial drugs is important for designing new
199 compound derivatives that can potentially improve inhibition of their molecular targets. To this end, at
200 least two critical pieces of information are required to achieve this goal – first is the identification of the
201 molecular targets inhibited by these drugs, and an equally important second step, is the high-
202 resolution structure of the drug bound to the molecular target to enable structure-guided drug design
203 to improve the potency of the drug for target inhibition. Here we have solved these problems for the
204 antimalarial MFQ by revealing the *P. falciparum* 80S ribosome as one of the targets of MFQ-mediated
205 parasite killing. In addition, a high-resolution cryo-EM structure of the Pf80S with bound (+)-MFQ
206 enantiomer presented in this study, along with proof of principle synthesizing of MFQ derivatives with
207 enhanced antimalarial activity, this body of work establishes the foundation for designing new MFQ
208 derivatives to inhibit parasite protein synthesis

209 The inhibition of Pf80S by MFQ is consistent with the known site of action of MFQ being in the
210 parasite cytoplasm. This has been demonstrated previously that the removal of MFQ from the parasite
211 cytoplasm into the food vacuole by the drug transporter Pgh-1 is the predominate basis for MFQ
212 resistance [7-10]. Furthermore, the mechanism of MFQ resistance in *P. falciparum* is inversely correlated
213 with chloroquine (CQ) resistance [8], suggesting that the primary mode of action of MFQ is not in the
214 parasite food vacuole, the compartment where CQ acts to inhibit heme polymerization. By solving the
215 structure of MFQ bound to the Pf80S, this has led to the identification of binding residues in the 28S
216 ribosomal RNA and protein PfuL13 that interact with the (+)-MFQ enantiomer. This site is part of the
217 GAC of the eukaryotic ribosome known for its important role in the polypeptide elongation step during
218 protein synthesis, suggesting this is the stage that (+)-MFQ inhibits. Importantly, CRISPR-cas9-
219 mediated amino acid substitution of (+)-MFQ binding residues in uL13 generated transgenic parasites
220 with increased drug resistance (highest EC50 = 43.8 nM: Table 1). The measured EC50s of these
221 transgenic parasites (36.6 – 43.8 nM) in response to MFQ treatment is within the range of published
222 EC50s measured in field isolates (mostly clustered within 35 - 60 nM) that have a MFQ resistance
223 profile [31]. It is important to note that the mechanism of MFQ resistance mediated by Pgh-1 in *P.*

224 *falciparum* is independent of the molecular target of the drug (mode of killing). Based on genetic
225 evidence from four independent single amino acid substitutions of PfuL13 with significantly higher
226 resistance to MFQ, (Fig 3c and Table 1), the data demonstrate that the Pf80S ribosome is at least one
227 of the targets of MFQ-mediated parasite killing.

228 Interestingly, the potency of MFQ in inhibiting parasite protein synthesis (55%) is relatively lower than
229 the highly toxic translation inhibitor CHX (90 %) (Fig. 1a). Mechanistically, CHX and MFQ work
230 distinctly based on the mode of their interactions with the ribosome. CHX competitively blocks the
231 binding of deacylated tRNA to the E-site of the 60S subunit [32], whilst on the contrary, binding of (+)-
232 MFQ to its primary binding site in the PfuL13 pocket of the GAC does not directly compete for binding
233 with any factors. This difference in the binding mode likely explains the variation in inhibition potency
234 of the two translation inhibitors with radically distinct modes of interaction with the 60S subunit. Similar
235 to other antibiotics such as thiopeptide and orthosomycin, (+)-MFQ also binds to the GAC of Pf60S
236 subunit. Although thiopeptide/orthosomycin utilize a different binding site within the GAC compared to
237 (+)-MFQ[19], nevertheless, (+)-MFQ would similarly be expected to function by inhibiting the polypeptide
238 elongation step during parasite protein synthesis. Furthermore, we have demonstrated the functional
239 importance of the PfuL13 MFQ pocket by introducing amino acid substitutions to residues that form
240 this pocket. By replacing Leu15 and Ile42 with Ser, this resulted in a lethal phenotype after
241 transfection, indicating the essential nature of this pocket of the GAC for generating viable parasites,
242 implying an essential function of the GAC for protein synthesis. Single amino acid substitutions to the
243 PfuL13 pocket with the resultant change in EC50s in response to MFQ treatment also demonstrate the
244 functional importance of this site of the GAC.

245 The nature of (+)-MFQ binding to the primary binding site is dominated by a number of hydrophobic
246 residues of PfuL13 that form this pocket (Leu15, Ile42, Tyr53, Phe56, Leu59, Leu140), whilst a charge
247 residue (Glu55) of PfuL13 and the sugar phosphate backbone of the 28S ribosomal RNA (G1441,
248 C1442) also contribute to (+)-MFQ binding. Importantly, comparison of uL13 between the human and
249 *P. falciparum* 80S ribosomes reveals significant differences exist in the MFQ pocket. This observation

provides a foundation for improving the potency of MFQ towards better inhibition of parasite protein synthesis. Two divergent residues in human and parasite uL13 (Glu55Ala and Leu59Lys *Pf:* human) are readily identifiable (Supplementary Fig. 6a), which form the basis for increasing the potency of (+)-MFQ on the parasite translation machinery. We have shown by introducing Glu55Ala that mimics the human ribosome increased the EC50 of this transgenic parasite from 26 nM to 38.3 nM compared to isogenic wild type control. We hypothesize that by an iterative optimization process, (+)-MFQ derivatives that effectively engage with Glu55 and Leu59 of the *P. falciparum* uL13 pocket may generate more potent compounds that inhibit parasite protein synthesis (Fig 4 and Table 1). Together with recent structural analyses of the Pf80S [14, 33] showing the many parasite specific features along with structural dynamics unique to the parasite ribosome, these data reinforce the idea that the *P. falciparum* 80S ribosome is an increasingly attractive target for antimalarial drug development. Although improving the potency of (+)-MFQ towards inhibition of parasite protein synthesis is important for the improvement of on-target inhibition, other factors such as safety concerns with MFQ-associated neurological toxicity due to off-target effects will also need to be overcome in order to develop second generation MFQ derivatives with clear clinical benefit over the parental form. Furthermore, noting that a 90 nM of MFQ (IC_{90}) concentration only inhibited translation by 55 % (Fig. 1a), this suggests other unidentified targets are likely to be inhibited by MFQ racemic mixture. Since the cryo-EM structure of the Pf80S-MFQ complex presented in this study shows the (+) form of MFQ enantiomer bound to the GTPase-associated center-PfuL13 pocket (Fig 2-3), this suggests that the (-) form of MFQ enantiomer may be a key factor inhibiting other molecular targets in the parasite.

The identification of MFQ as a protein synthesis inhibitor raises the question of whether other related antimalarials such as quinine (QN) and lumefantrine (LF) may also inhibit parasite protein synthesis through the PfuL13 pocket. Although these compounds have a related chemical scaffold, the substantial alterations in their structure would argue against their ability to interact with the PfuL13 MFQ pocket. Further biochemical characterization of QN and LF would be required to determine their effect on parasite protein synthesis.

Finally, in this study we have demonstrated how cryo-EM can function as an attractive tool for the development of MFQ-based improved protein-synthesis inhibitors. The low yield of Pf80S using cultured parasites has so far precluded the ability to crystalize the Pf80S for structural studies of drug interaction, although sufficient ribosome material may now be feasible for use in biological assays [34]. Together with recent elucidation of the structure of the Pf80S-emetine complex [14], cryo-EM is now the method of choice for the design of new inhibitors to the Pf80S ribosome.

REFERENCES

1. World Malaria Report (WHO, 2016).
2. White, N.J. et al. Malaria. *Lancet* **383**, 723-35 (2014).
3. Wells, T.N., Hooft van Huijsduijnen, R. & Van Voorhis, W.C. Malaria medicines: a glass half full? *Nat Rev Drug Discov* **14**, 424-42 (2015).
4. Nevin, R.L. & Byrd, A.M. Neuropsychiatric Adverse Reactions to Mefloquine: a Systematic Comparison of Prescribing and Patient Safety Guidance in the US, UK, Ireland, Australia, New Zealand, and Canada. *Neurol Ther* **5**, 69-83 (2016).
5. Lim, P. et al. Decreasing pfmdr1 copy number suggests that Plasmodium falciparum in Western Cambodia is regaining in vitro susceptibility to mefloquine. *Antimicrob Agents Chemother* **59**, 2934-7 (2015).
6. Roberts, L. Malaria wars. *Sci Transl Med* **352**, 398-405 (2016).
7. Sanchez, C.P., Rotmann, A., Stein, W.D. & Lanzer, M. Polymorphisms within PfMDR1 alter the substrate specificity for anti-malarial drugs in Plasmodium falciparum. *Mol Microbiol* **70**, 786-98 (2008).
8. Cowman, A.F., Galatis, D. & Thompson, J.K. Selection for mefloquine resistance in Plasmodium falciparum is linked to amplification of the pfmdr1 gene and cross-resistance to halofantrine and quinine. *Proc Natl Acad Sci U S A* **91**, 1143-7 (1994).
9. Reed, M.B., Saliba, K.J., Caruana, S.R., Kirk, K. & Cowman, A.F. Pgh1 modulates sensitivity and resistance to multiple antimalarials in Plasmodium falciparum. *Nature* **403**, 906-9. (2000).
10. Sanchez, C.P., Dave, A., Stein, W.D. & Lanzer, M. Transporters as mediators of drug resistance in Plasmodium falciparum. *Int J Parasitol* **40**, 1109-18 (2010).
11. Gamo, F.-J. et al. Thousands of chemical starting points for antimalarial lead identification. *Nature* **465**, 305-10 (2010).
12. Dahl, E.L. et al. Tetracyclines specifically target the apicoplast of the malaria parasite Plasmodium falciparum. *Antimicrob Agents Chemother* **50**, 3124-31 (2006).
13. Goodman, C.D., Su, V. & McFadden, G.I. The effects of anti-bacterials on the malaria parasite Plasmodium falciparum. *Mol Biochem Parasitol* **152**, 181-91 (2007).
14. Wong, W. et al. Cryo-EM structure of the Plasmodium falciparum 80S ribosome bound to the anti-protozoan drug emetine. *Elife*, e03080 (2014).
15. Ben-Shem, A. et al. The structure of the eukaryotic ribosome at 3.0 A resolution. *Science* **334**, 1524-9 (2011).

16. Spahn, C.M. et al. Domain movements of elongation factor eEF2 and the eukaryotic 80S ribosome facilitate tRNA translocation. *EMBO J* **23**, 1008-19 (2004).
17. Brodersen, D.E. et al. The structural basis for the action of the antibiotics tetracycline, pactamycin, and hygromycin B on the 30S ribosomal subunit. *Cell* **103**, 1143-54 (2000).
18. Ohnmacht, C.J., Patel, A.R. & Lutz, R.E. Antimalarials. 7. Bis(trifluoromethyl)- -(2-piperidyl)-4-quinolinemethanols. *J Med Chem* **14**, 926-8 (1971).
19. Harms, J.M. et al. Translational regulation via L11: molecular switches on the ribosome turned on and off by thiostrepton and micrococcin. *Mol Cell* **30**, 26-38 (2008).
20. Ghorbal, M. et al. Genome editing in the human malaria parasite Plasmodium falciparum using the CRISPR-Cas9 system. *Nature biotechnology* **32**, 819-21 (2014).
21. Lelievre, J. et al. Activity of clinically relevant antimalarial drugs on Plasmodium falciparum mature gametocytes in an ATP bioluminescence "transmission blocking" assay. *PLoS One* **7**, e35019 (2012).
22. Delves, M.J. et al. Male and female Plasmodium falciparum mature gametocytes show different responses to antimalarial drugs. *Antimicrob Agents Chemother* **57**, 3268-74 (2013).
23. Waters, A.P., Syin, C. & McCutchan, T.F. Developmental regulation of stage-specific ribosome populations in Plasmodium. *Nature* **342**, 438-40 (1989).
24. Aguiar, A.C., Pereira, D.B., Amaral, N.S., De Marco, L. & Krettli, A.U. Plasmodium vivax and Plasmodium falciparum ex vivo susceptibility to anti-malarials and gene characterization in Rondonia, West Amazon, Brazil. *Malar J* **13**, 73 (2014).
25. Otigbuo, I.N. & Onabanjo, A.O. The in vitro and in vivo effects of mefloquine on Trypanosoma brucei brucei. *J Hyg Epidemiol Microbiol Immunol* **36**, 191-9 (1992).
26. Holfels, E., McAuley, J., Mack, D., Milhous, W.K. & McLeod, R. In vitro effects of artemisinin ether, cycloguanil hydrochloride (alone and in combination with sulfadiazine), quinine sulfate, mefloquine, primaquine phosphate, trifluoperazine hydrochloride, and verapamil on Toxoplasma gondii. *Antimicrob Agents Chemother* **38**, 1392-6 (1994).
27. Khatter, H., Myasnikov, A.G., Natchiar, S.K. & Klaholz, B.P. Structure of the human 80S ribosome. *Nature* **520**, 640-5 (2015).
28. Brown, A. et al. Structure of the large ribosomal subunit from human mitochondria. *Science* **346**, 718-22 (2014).
29. Milner, E. et al. Structure-activity relationships amongst 4-position quinoline methanol antimalarials that inhibit the growth of drug sensitive and resistant strains of Plasmodium falciparum. *Bioorg Med Chem Lett* **20**, 1347-51 (2010).
30. Milner, E. et al. Anti-malarial activity of a non-piperidine library of next-generation quinoline methanols. *Malar J* **9**, 51 (2010).
31. Na-Bangchang, K., Muhamad, P., Ruaengweerayut, R., Chaijaroenkul, W. & Karbwang, J. Identification of resistance of Plasmodium falciparum to artesunate-mefloquine combination in an area along the Thai-Myanmar border: integration of clinico-parasitological response, systemic drug exposure, and in vitro parasite sensitivity. *Malar J* **12**, 263 (2013).
32. Garreau de Loubresse, N. et al. Structural basis for the inhibition of the eukaryotic ribosome. *Nature* **513**, 517-22 (2014).
33. Sun, M. et al. Dynamical features of the Plasmodium falciparum ribosome during translation. *Nucleic Acids Res* (2015).
34. Ahyong, V. et al. Identification of Plasmodium falciparum specific translation inhibitors from the MMV Malaria Box using a high throughput in vitro translation screen. *Malar J* **15**, 173 (2016).
35. Mindell, J.A. & Grigorieff, N. Accurate determination of local defocus and specimen tilt in electron microscopy. *J Struct Biol* **142**, 334-47 (2003).

36. Scheres, S.H. RELION: implementation of a Bayesian approach to cryo-EM structure determination. *J Struct Biol* **180**, 519-30 (2012).
37. Bai, X.C., Fernandez, I.S., McMullan, G. & Scheres, S.H. Ribosome structures to near-atomic resolution from thirty thousand cryo-EM particles. *Elife* **2**, e00461 (2013).
38. Scheres, S.H. Beam-induced motion correction for sub-megadalton cryo-EM particles. *Elife* **3**, e03665 (2014).
39. Chen, S. et al. High-resolution noise substitution to measure overfitting and validate resolution in 3D structure determination by single particle electron cryomicroscopy. *Ultramicroscopy* **135**, 24-35 (2013).
40. Rosenthal, P.B. & Henderson, R. Optimal determination of particle orientation, absolute hand, and contrast loss in single-particle electron cryomicroscopy. *J Mol Biol* **333**, 721-45 (2003).
41. Kucukelbir, A., Sigworth, F.J. & Tagare, H.D. Quantifying the local resolution of cryo-EM density maps. *Nat Methods* **11**, 63-5 (2014).
42. Emsley, P., Lohkamp, B., Scott, W.G. & Cowtan, K. Features and development of Coot. *Acta Crystallogr D Biol Crystallogr* **66**, 486-501 (2010).
43. Murshudov, G.N. et al. REFMAC5 for the refinement of macromolecular crystal structures. *Acta Crystallogr D Biol Crystallogr* **67**, 355-67 (2011).
44. Amunts, A. et al. Structure of the yeast mitochondrial large ribosomal subunit. *Science* **343**, 1485-9 (2014).
45. Nicholls, R.A., Long, F. & Murshudov, G.N. Low-resolution refinement tools in REFMAC5. *Acta Crystallogr D Biol Crystallogr* **68**, 404-17 (2012).
46. Chou, F.C., Sripakdeevong, P., Dibrov, S.M., Hermann, T. & Das, R. Correcting pervasive errors in RNA crystallography through enumerative structure prediction. *Nat Methods* **10**, 74-6 (2013).
47. Chen, V.B. et al. MolProbity: all-atom structure validation for macromolecular crystallography. *Acta Crystallogr D Biol Crystallogr* **66**, 12-21 (2010).
48. Baum, J. et al. Reticulocyte-binding protein homologue 5 - An essential adhesin involved in invasion of human erythrocytes by Plasmodium falciparum. *Int J Parasitol* **39**, 371-80 (2009).
49. Boyle, M.J. et al. Isolation of viable Plasmodium falciparum merozoites to define erythrocyte invasion events and advance vaccine and drug development. *Proc Natl Acad Sci USA* **107**, 14378-83 (2010).
50. US Patent (2003) US6608085 4-quinolinemethanol derivatives as purine receptor antagonists (II).

Additional information

Supplementary information is available online. Reprints and permission information is available online at www.nature.com/reprints. Correspondence and requests for materials should be addressed to S.H.W.S and J.B.

ACKNOWLEDGEMENTS

We thank, I. Lucet, J. Boddey, S. Herrmann, G. McFadden, J. Rayner, A. Ruecker, M. Delves, H. Baumann, G. Murshudov and P. Emsley for helpful discussions and experimental assistance; S. Chen and C. Savva for help with microscopy; and J. Grimmett and T. Darling for help with computing. Experimental data presented here was made possible through Victorian State Government Operational Infrastructure Support and Australian Government NHMRC IRIISS. The research was directly supported by a National Health and Medical Research Council of Australia (NHMRC) Project Grant (APP1024678 J.B. & W.W.), the Australian Cancer Research Foundation, Human Frontier Science Program (HFSP) Young Investigator Program Grant (J.B. RGY0071/2011) and grants from the UK Medical Research Council (MC_UPA0251013 to S.H.W.S.). W.W. is an Early Career Development Awardee (APP1053801) from the NHMRC and was in receipt of a travel award from OzEMalaR to visit the MRC-LMB UK to conduct experiments. X.C.B. is supported by an EU FP7 Marie Curie Postdoctoral Fellowship. A.B. and I.F. are supported by grants to V. Ramakrishnan from the Wellcome Trust (WT096570) and the UK Medical Research council (MC_U105184332). J.B. was supported through a Future Fellowship (FT100100112) from the Australian Research Council (ARC) and is currently supported by an Investigator Award from the Wellcome Trust (100993/Z/13/Z), with additional support for this work coming from a Pathfinder Award from the Wellcome Trust (105686).

Author Contributions: W.W., X-C.B., B.E.S., K.E.J, T.T., D.S.M., S.A.R, S.H.W.S and J.B. designed all experiments; W.W., X-C.B, B.E.S., K.E.J, A.B., T.T., D.S.M., J.K.T., E.H. and I.S.F. performed experiments; W.W., X-C.B, B.E.S., K.E.J., T.T., A.B., J.K.T., S.A.R., A.F.C., S.H.W.S. and J.B. contributed to manuscript preparation.

Competing interests:

The authors declare no competing financial interests.

Table 1: Antimalarial activity of mefloquine and derivatives.

Drug	Strain tested	EC_{50} (nM)	*P* value
MFQ	3D7	25.3 ± 3.4	-
MFQ	3D7.transgenic Wild Type uL13	26.0 ± 1.2	-
MFQ	3D7.uL13.I42A	39.9 ± 5.6	**0.0314**[a]
MFQ	3D7.uL13.E55A	38.3 ± 4.0	**0.0218**[a]
MFQ	3D7.uL13.F56A	43.8 ± 6.4	**0.0243**[a]
MFQ	3D7.uL13.L140F	36.6 ± 5.3	**0.0442**[a]
MFQ_D1	3D7	12.4 ± 4.5	0.0588[b]
MFQ_D2	3D7	40.9 ± 10.8	0.0771[b]
MFQ_D3	3D7	11.1 ± 1.1	**0.0251**[b]
MFQ_D4	3D7	13.3 ± 2.4	**0.0433**[b]
MFQ_D5	3D7	10.6 ± 3.6	**0.0367**[b]
MFQ_D6	3D7	15.8 ± 2.3	0.0671[b]
MFQ_D7	3D7	15.6 ± 2.7	0.0676[b]

[a] Comparisons of EC_{50} of transgenic parasites with L13 variants to transgenic parasite with wild type L13.
[b] Comparisons of EC_{50} of 3D7 parasites treated with MFQ-derivatives to MFQ control.
Boldface indicates a statistically significant difference indicated by *P*-values calculated by the t-test.

FIGURE LEGENDS

Figure 1 | MFQ inhibits cytosolic translation in *P. falciparum*. a, Translation inhibitory activity of antimalarial compounds, cycloheximide (CHX) at 1.3 μM, doxycycline (DOX) at 17 μM, chloroquine (CQ) at 110 nM, emetine (EME) at 105 nM and mefloquine (MFQ) at 90 nM. Statistical significance was calculated by t-test. Mean ± SD are shown. Each assay was undertaken in triplicate of four independent occasions. **b,** Chemical structure of MFQ.

Figure 2 | MFQ interacts with the GTPase-associated center of the *P. falciparum* large ribosomal subunit. a-b, Cryo-EM density map of the primary MFQ binding pocket in the absence **(a)** and presence of MFQ **(b)**. MFQ is represented as yellow sticks and binding residues are in purple. Oxygen is in red, nitrogen in blue, fluorine in cyan, and magnesium in green. **c,** Magnified EM density of (+)-MFQ depicted in various orientations. **d,** Ribosomal protein PfuL13 and rRNA ES13 form the MFQ binding pocket. Hydrophobic residues are colored in gray. Structure is derived from 112,347 particles from 829 micrographs (see Supplementary information). **e,** Atomic model of the Pf80S-MFQ

complex is shown from the A-site entry side. Magnified inset shows the composition of the GTPase-associated center (GAC) with bound MFQ.

Figure 3 | The primary binding site for (+)-MFQ. a, Amino acid residues from the protein PfuL13 and bases from ES13 of the 28S rRNA involved in binding to (+)-MFQ. **b,** Residues that interact with (+)-MFQ with inter-atomic distances indicated. **c,** Mefloquine-mediated growth inhibition of control *P. falciparum* parasites carrying an integrated, wild type copy of uL13 gene and four transgenic parasite lines carrying single amino acid substitutions at the uL13 MFQ binding pocket. Data are shown as the mean ± SD of three biological replicates with each biological replicate representing three experimental replicates. **d,** Divergence in the ES13 part of the MFQ binding pocket between the *P. falciparum* A type (blood stage) and S type (sexual stage) ribosomes. A single nucleotide C1440 in the A-type 28S rRNA is deleted in the S-type 28S rRNA. MFQ binding residues are highlighted in a box. **e,** Sequence alignment of uL13 from *P. falciparum, P. vivax, T. gondii* and *T. brucei.* Residues involved in binding to MFQ are highlighted with asterisks.

Figure 4 | Structure based design of MFQ-derivatives. a, Chemical structure of MFQ_D1. **b,** MFQ_D1 docked into the MFQ binding pocket. **c,** Chemical structure of MFQ_D2. **d,** MFQ_D2 docked into the MFQ pocket. **e,** Parasite growth inhibition assay measuring the inhibitory activity of MFQ derivatives on 3D7 parasites. Data are shown as the mean ± SD of three biological replicates with each biological replicate representing three experimental replicates.

METHODS

Parasite culture and ribosome purification

Wild type 3D7 strain of *P. falciparum* parasites, a clone itself derived from NF54, provided by the late David Walliker at Edinburgh University, UK were maintained in human erythrocytes (blood group O) at a hematocrit of 4% with 10% Albumax. Saponin lysed parasite pellets were incubated with lysis buffer (20 mM Hepes, pH 7.4, 250 mM KCl, 25 mM $Mg(Ac)_2$, 0.15 % Triton, 5 mM 2-mecaptoethanol) at 4°C for 1 hr. Ribosomes were purified by ultracentrifugation initially with a sucrose cushion (20 mM Hepes pH 7.4, 1.1 M sucrose, 40 mM KAc, 10 mM NH_4Ac, 10 mM $Mg(Ac)_2$ and 5 mM 2-mecaptoethanol) followed by a 10-40 % sucrose gradient separation step using the same buffer.

Drug sensitivity assay

Trophozoite stage parasites at 0.5% parasitemia were grown in a 50 µl culture at 2% hematocrit in 96 well round bottom microtitre plates (Falcon) with doubling dilutions of each drug. After incubation for 48 hours each well was fixed at room temperature for 30 minutes with 50 ul of 0.25% glutaraldehyde (ProSciTech) diluted in PBS. Following centrifugation at 1,200 rpm for 2 mins, supernatants were discarded and trophozoite stage parasites were stained with 50 µl of 5X SYBR Green (Invitrogen) diluted in PBS. The parasitemia of each well was determined by counting 50,000 cells by flow cytometry using a Cell Lab Quanta SC – MPL Flow Cytometer (Beckman Coulter). Growth was expressed as a percentage of the parasitemia obtained using a drug-free control. All samples were tested in triplicate.

Parasite translation assay

Synchronous trophozoite-stage 3D7 parasites were dispensed into a 24-well plate to a final parasitaemia of 4-6%, 2% haematocrit with IC90 concentrations of chloroquine (110 nM), cycloheximide (1.3 µM), doxycycline (17 µM), emetine (105 nM or mefloquine (90nM) in a final volume of 1 mL. Parasites were cultured for 2 hr at 37 °C in a humidified atmosphere of 5% CO_2, 1% O_2 and

94% N_2. Following the 2 hr incubation, 800 µL aliquots were transferred to rubber-sealed 1.5 mL tubes to which 16.5 µCi EasyTag(TM) EXPRE35S35S Protein Labeling Mix, [3S] (PerkinElmer) was added and incubated for 2hr at 37 °C in growth media made from RPMI HEPES lacking L-cysteine and L-methionine. Infected erythrocytes were washed twice with 1xPBS, resuspended in 6x protein sample loading buffer and proteins separated by SDS-PAGE. Gels were fixed (40% (v/v) methanol and 10% (v/v) acetic acid) for 15min and stained with Invitrogen SimplyBlue Safe Stain as per manufacturer's instructions. Gels were dried between cellophane, exposed to a phosphor plate for 3days and imaged with a GE Typhoon phosphorimager. Densitometric analysis was performed using ImageJ software. Experiments were conducted four times independently.

Electron microscopy

Aliquots of 3 µl of purified Pf80S at a concentration of ~160 nM were incubated with a 2 mM solution of MFQ (BioBlocks Inc,) in 20 mM Hepes pH7.4, 40 mM KAc, 10 mM NH_4Ac, 10 mM $Mg(Ac)_2$ and 5 mM 2-mecaptoethanol for 15 minutes at 25 °C. Samples were incubated for 30 s on glow-discharged holey carbon grids (Quantifoil R1.2/1.3), on which a home-made continuous carbon film (estimated to be ~30 Å thick) had previously been deposited. Grids were blotted for 2.5 s and flash frozen in liquid ethane using an FEI Vitrobot. Pf80S-MFQ grids were transferred to an FEI Tecnai Polara electron microscope that was operated at 300 kV. Images were recorded manually during two non-consecutive days on a back-thinned FEI Falcon II detector at a calibrated magnification of 104,478 (yielding a pixel size of 1.34 Å). Defocus values in the final data set ranged from 1.0 - 3.3 µm. During the data collection sessions, all images that showed signs of significant a stigmatism or drift were discarded. An in-house built system was used to intercept the videos frames from the detector at a rate of 16 s^{-1}.

Image processing

We used RELION (version 1.3-beta) for automated selection of 112,347 particles from 829

534 micrographs for the Pf80S-MFQ sample. Contrast transfer function parameters were estimated using
535 CTFFIND3[35]. All 2D and 3D classifications and refinements were performed using RELION[36]. We used
536 reference-free 2D class averaging and 3D classification to discard suboptimal particles. A 60 Å low-
537 pass filtered cryo-EM reconstruction of the *P. falciparum* 80S ribosome (EMDB-2661[14]) was used as
538 an initial model for the 3D refinement. The final refinement for the Pf80S-MFQ sample contained
539 43,184 particles.
540
541 For the correction of beam-induced movements, we used statistical movie processing as described
542 previously[37], with running averages of five movie frames, and a standard deviation of 1 pixel for the
543 translational alignment. To further increase the accuracy of the movement correction, we used
544 RELION particle polishing to fit linear tracks through the optimal translations for all running averages[38],
545 and included neighboring particles on the micrograph in these fits. In addition, we employed a
546 resolution and dose-dependent model for the radiation damage, where each frame is weighted with a
547 different B-factor as was estimated from single-frame reconstructions. These procedures yielded a
548 map with an overall resolution of 3.2 Å for the Pf80S-MFQ complex.
549
550 Reported resolutions are based on the gold-standard FSC=0.143 criterion[39], and were corrected for
551 the effects of a soft mask on the FSC curve using high-resolution noise substitution[39]. Prior to
552 visualization, all density maps were corrected for the modulation transfer function (MTF) of the
553 detector, and then sharpened by applying a negative B-factor (Supplementary Data Table 1) that was
554 estimated using automated procedures[40].
555
556 In order to locate MFQ in the Pf80S-MFQ reconstruction, we calculated a difference map between the
557 reconstructions of empty Pf80S[14] and Pf80S-MFQ. To this purpose, the two MTF-corrected and B-
558 factor sharpened maps were aligned with respect to each other using the "*Fit in Map*" functionality in
559 UCSF Chimera 7. Piror to subtraction, the empty Pf80S map was re-interpolated on the Cartesian grid
560 of the Pf80S-MFQ map and the power spectrum of the empty Pf80S map was re-scaled to match the

power spectrum of the Pf80S-MFQ map. For visualization purposes, the resulting difference map was low-pass filtered at 4 Å and the threshold was set at 5 standard deviations as calculated within the area of the Pf80S ribosome (Supplementary Fig. 3). At this threshold, only two continuous density features were visible. The highest difference density inside these features extended to 6.5 and 9.3 standard deviations in the difference map for the primary and secondary sites, respectively.

Local resolution variations in the reconstruction was estimated using ResMap[41]. To improve the resolution of the Pf80S-MFQ reconstruction, a "focused" refinement was performed, where we masked out the large subunit at every iteration. This generated a map (Supplementary Fig. 2) with improved density for the large ribosomal subunit (at an overall resolution of 3.2 Å), and this map was used for the refinement of the atomic model as described below.

Model building and refinement

The available Pf60S atomic model (PDB accession code 3J79[14]) was used as a starting model for the refinement of the Pf80S-MFQ reconstruction. MFQ was first real space refined in Coot[42] and the model was subsequently stereo-chemically refined using REFMAC v.5.8, which was modified for structures determined by cryo-EM[43, 44]. The *Pf*60S-MFQ atomic model was refined in the map that was obtained in the focused refinement of the cryo-EM reconstruction. Structure factors for the (reciprocal-space) refinement in REFMAC were obtained by cutting out sections of the corresponding maps with a 3 Å radius from the center of each atom in the model. Structure factor phases were not altered during refinement.

Throughout refinement, reference and secondary structure restraints were applied to the ribosomal proteins using the Sc80S structure as a reference model[45]. Base pair and parallelization restraints obtained using LIBG were also applied throughout refinement[44]. The stereochemistry of the rRNA model was further improved using the ERRASER-PHENIX pipeline[46]. Ramachandran restraints were not applied during refinement to preserve backbone dihedral angles for validation.

588

589 The average overall Fourier shell correlation (FSCaverage) was monitored during refinement
590 (Supplementary Data Table 1) and the final model was validated using MolProbity[47]. For cross-
591 validation against over-fitting we randomly displaced the atoms of our final model (with an r.m.s.d. of
592 0.5 Å), and performed a fully restrained refinement against a map that was reconstructed from only
593 one of the two independent halves of the data that were used in our gold-standard FSC procedure.
594 We then calculated FSC curves between the resulting model and the half-map against which it had
595 been refined (FSCwork), as well as the FSC curve between that model and the other half-map
596 (FSCtest). The observation that the FSCwork and FSCtest curves overlap demonstrates the absence
597 of overfitting of the model (Supplementary Fig. 2b).

598

599 **CRISPR mutagenesis of PfuL13.**

600 **Cas9-expressing plasmid**. The DHOD selectable marker was removed from the pUF1-cas9
601 plasmid[20], by self-ligating the XbaI/SpeI-cut plasmid. Then a NcoI/AatII fragment containing the cas9-
602 gRNA cassette was removed from the pL6-eGFP plasmid[20] and cloned into the pUF1-cas9 plasmid
603 lacking DHOD above, resulting in the pUF1-cas9-gRNA plasmid. The 20 nucleotide guide sequence
604 (GAATATGTTATCGATTGCAA) was cloned into the BtgZI sites of this plasmid using the In-Fusion
605 method (Clontech, USA).

606

607 **HDR plasmids.** The plasmids for homology directed repair were assembled in the p1.2 plasmid used
608 to tag genes at the 3' end with Strep II and 3HA tags[48]. The 5' homology flanks were synthesized
609 (Geneart, Germany), as the 5' portion of the recodoned uL13 sequence (Supplementary Data Table
610 3). The 3' homology flank was amplified using primers p9 and p10 (Supplementary Table 2) and
611 cloned into the EcoRI/KasI sites of the p1.2 plasmid. Subsequently, the 5' flanks bounded by
612 BglII/XhoI sites (Supplementary Table 3) were cloned into the 3' flank-containing p1.2 plasmid. This
613 resulted in 6 plasmids encoding either wild-type (wt), L15S/I42S, I42A, E55A, F56A or L140F uL13
614 genes.

615

616 **Transfection.** E64-treated magnet-purified schizonts[49] were transfected with 100ug circular guide-
617 containing plasmid and 50ug of each of the 6 linearized plasmids containing the homology flanks.. A
618 Nucleofector 1 device was used as per the manufacturer's protocol (Amaxa, Germany). Cultures were
619 selected with WR99210.

620

621 **General chemistry methods**

622 Analytical thin-layer chromatography was performed on Merck silica gel 60F254 aluminum-backed
623 plates and were visualized by fluorescence quenching under UV light. Flash chromatography was
624 performed with silica gel 60 (particle size 0.040-0.063 □m). NMR spectra were recorded on a Bruker
625 Avance DRX 300 (^{1}H NMR at 300 MHz) with the solvents indicated. Chemical shifts are reported in
626 ppm on the δ scale and referenced to the appropriate solvent peak. HRESMS were acquired by Jason
627 Dang at the Monash Institute of Pharmaceutical Sciences Spectrometry Facility using an Agilent 1290
628 infinity 6224 TOF LCMS. Column used was RRHT 2.1 x 50 mm 1.8 µm C18. Gradient was applied
629 over the 5 min with the flow rate of 0.5 mL/min. For MS: Gas temperature was 325^{o}C; drying gas 11
630 L/min; nebulizer 45 psig and the fragmentor 125V. LCMS were recorded on a Waters ZQ 3100 using a
631 2996 Diode Array Detector. LCMS conditions used to assess purity of compounds were as follows,
632 column: XBridge TM C18 5 µm 4.6 x100 mm, injection volume 10 µL, gradient: 10-100% B over 10
633 min (solvent A: water 0.1% formic acid; solvent B: AcCN 0.1% formic acid), flow rate: 1.5 mL/min,
634 detection: 100-600 nm. All final compounds were analyzed using ultrahigh performance liquid
635 chromatography/ultraviolet/evaporative light scattering detection coupled to mass spectrometry.
636 Unless otherwise noted, all compounds were found to be >95% pure by this method. 2-[2,8-
637 Bis(trifluoromethyl)-4-quinolyl]oxirane was purchased commercially and used without further
638 purification.

639

640 **Synthesis of MFQ analogues**

641 The MFQ analogues, MFQ_D1 and MFQ_D2, were generated according to the method by Milner *et*

al.[29, 30]

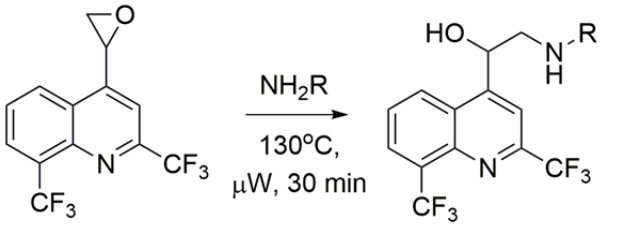

Scheme 1. Synthesis of MFQ analogues.

General Procedure A. 4-(Oxiran-2-yl)-2,8-bis(trifluoromethyl)quinoline (30 mg, 0.10 mmol) and the appropriate amine (0.49 mmol) in *i*PrOH (2 mL) were irradiated in a CEM microwave reactor for 30 min at 130 °C. The reaction mixture was concentrated *in vacuo* and purified by silica chromatography gradient eluting with 100% DCM to 7.5% MeOH/DCM/0.1% NH_4OH to obtain the amino quinoline.

1-(2,8-Bis(trifluoromethyl)quinolin-4-yl)-2-(cyclohexylamino)ethanol (MFQ_D1).

General Procedure A was followed using cyclohexylamine (56 μL, 0.49 mmol) to obtain MFQ_D1 as a solid (30 mg, 76%). ^{1}H NMR ($CDCl_3$): δ 8.27 (d, *J* = 8.3 Hz, 1H), 8.19-8.14 (m, 2H), 7.73 (t, *J* = 8.1 Hz, 1H), 5.50 (dd, *J* = 8.6 and 3.3 Hz, 1H), 3.29 (dd, *J* = 12.5 and 3.8 Hz, 1H), 2.76-2.50 (m, 3H), 1.97-1.93 (m, 2H), 1.79-1.64 (m, 3H), 1.31-1.10 (m, 5H). ^{13}C NMR (75 MHz, $CDCl_3$) δ 151.6, 148.9, 148.4, 143.7, 129.8, 128.7, 127.0, 125.3, 123.0, 121.7, 119.4, 114.5, 67.8, 56.7, 52.6, 34.1, 33.7, 25.9, 24.9. MS, *m/z* = 407 $[M + H]^+$. HRMS found: (M+H) 407.1561; $C_{19}H_{21}F_6N_2O$ requires (M+H), 407.1558.

1-(2,8-Bis(trifluoromethyl)quinolin-4-yl)-2-((2,3-dihydro-1H-inden-2-yl)amino)ethanol (MFQ_D2)

General Procedure A was followed using 2-aminoindane (64 μL, 0.49 mmol) to obtain MFQ_D2 as a solid (35 mg, 81%). ^{1}H NMR ($CDCl_3$): δ 8.23-8.17 (m, 2H), 8.14 (s, 1H), 7.75 (t, *J* = 7.8 Hz, 1H), 7.22-7.17 (m, 4H), 5.50 (dd, *J* = 8.9 and 3.3 Hz, 1H), 3.76-3.68 (m, 1H), 3.33-3.19 (m, 3H), 2.88-2.74 (m, 3H). ^{13}C NMR (75 MHz, $CDCl_3$) δ 151.2, 148.8, 148.4, 143.7, 141.0, 129.9, 129.5, 128.7, 127.1, 126.7,

125.3, 123.1, 121.7, 119.4, 114.5, 67.9, 59.3, 53.9, 40.2. MS, *m/z* = 441 $[M + H]^+$. HRMS found: (M+H) 441.1403; $C_{22}H_{19}F_6N_2O$ requires (M+H), 441.1402.

Mefloquine derivatives in Supplementary Data Table 4.

The MFQ analogues, MFQ_D3 to MFQ_D7, were generated according to the method by Milner *et al.*[29, 30]

1-(2,8-Bis(trifluoromethyl)quinolin-4-yl)-2-(isobutylamino)ethanol (MFQ_D3)

General Procedure A was followed using isobutylamine (49 μL, 0.49 mmol) to obtain MFQ_D3 as a solid (21 mg, 55%). This compound has data identical to that previously described.[50]

1-(2,8-Bis(trifluoromethyl)quinolin-4-yl)-2-(butylamino)ethanol (MFQ_D4)

General Procedure A was followed using n-butylamine (48 μL, 0.49 mmol) to obtain MFQ_D4 as a solid (29 mg, 76%). ^{1}H NMR ($CDCl_3$): δ 8.27 (d, *J* = 8.6 Hz, 1H), 8.19-8.14 (m, 2H), 7.73 (t, *J* = 7.9 Hz, 1H), 5.5-5.52 (m, 1H), 3.19 (dd, *J* = 12.5 and 3.5 Hz, 1H), 2.79-2.69 (m, 2H), 1.57-1.38 (m, 4H), 0.97-0.93 (m, 3H). MS, *m/z* = 381 $[M + H]^+$.

1-(2,8-Bis(trifluoromethyl)quinolin-4-yl)-2-((2-methylbutyl)amino)ethanol (MFQ_D5)

General Procedure A was followed using 2-methylbutylamine (58 μL, 0.49 mmol) to obtain MFQ_D5 as a solid (31 mg, 79%). This compound has data identical to that previously described.[29]

1-(2,8-Bis(trifluoromethyl)quinolin-4-yl)-2-(isopentylamino)ethanol (MFQ_D6)

General Procedure A was followed using isopentylamine (57 μL, 0.49 mmol) to obtain MFQ_D6 as a solid (32 mg, 82%). ^{1}H NMR ($CDCl_3$): δ 8.25-8.14 (m, 3H), 7.73 (t, *J* = 7.9 Hz, 1H), 5.54-5.49 (m, 1H), 3.24-3.17 (m, 1H), 2.83-2.64 (m, 2H), 1.70-1.65 (m, 2H), 1.47-1.40 (0.94-0.93 (m, 6H). MS, *m/z* = 395 $[M + H]^+$.

1-(2,8-Bis(trifluoromethyl)quinolin-4-yl)-2-(cyclopentylamino)ethanol (MFQ_D7)

General Procedure A was followed using cyclopentylamine (48 μL, 0.49 mmol) to obtain MFQ_D7 as a solid (31 mg, 79%). ^{1}H NMR ($CDCl_3$): δ 8.27 (d, *J* = 8.4 Hz, 1H), 8.19-8.14 (m, 2H), 7.73 (t, *J* = 8.0 Hz, 1H), 5.53 (dd, *J* = 8.9 and 3.5 Hz, 1H), 3.26-3.17 (m, 2H), 2.76-2.69 (m, 1H), 1.92-1.38 (m, 8H). MS, *m/z* = 393 $[M + H]^+$.

Data Availability: The data that support the findings of this study are available from the corresponding authors upon request. Structures are accessible via accession codes: A cryo-EM density map has been deposited in the Electron Microscopy Data Bank with accession number EMD-8576; and atomic coordinates have been deposited in the Protein Data Bank, with entry code 5UMD.

Figure 1

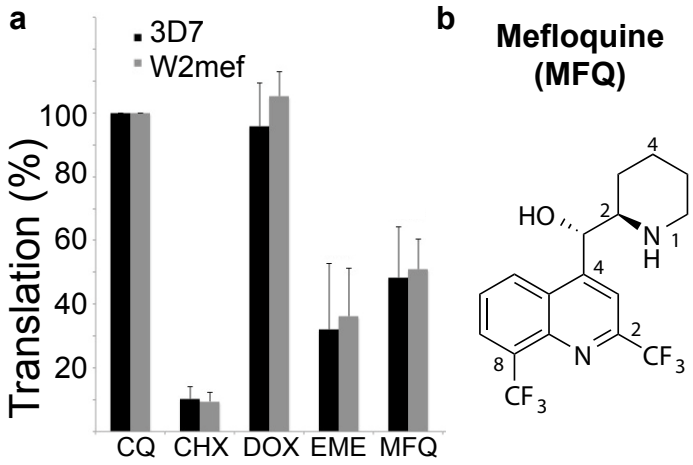
a
3D7
W2mef
Translation (%)
100
80
60
40
20
CQ
CHX
DOX
EME
MFQ
b
Mefloquine
(MFQ)
HO
N
H
N
CF3
CF3

Figure 2

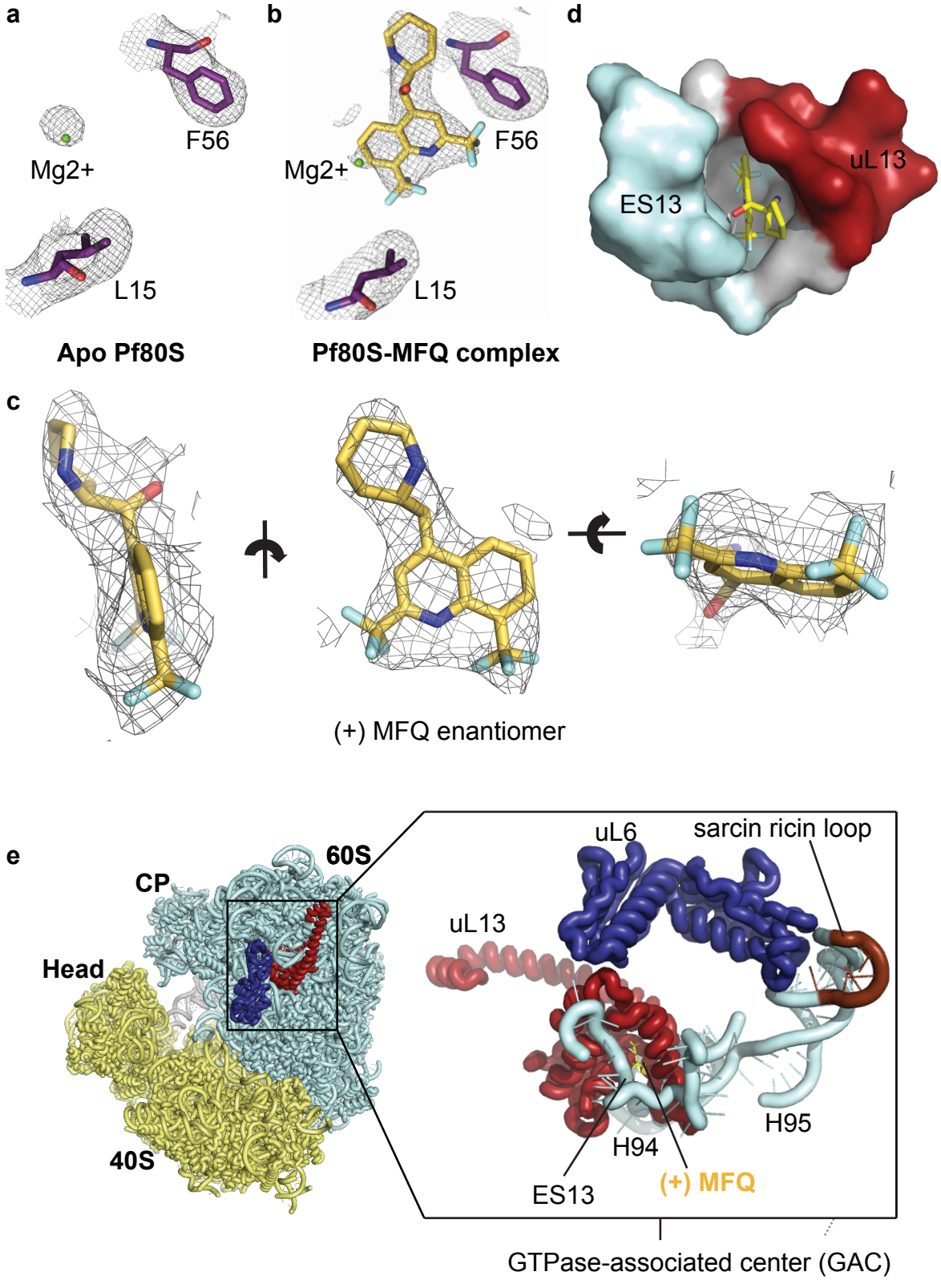
a
F56
Mg2+
L15
Apo Pf80S
b
F56
Mg2+
L15
Pf80S-MFQ complex
d
uL13
ES13
c
(+) MFQ enantiomer
e
60S
CP
Head
40S
uL6
sarcin ricin loop
uL13
H95
H94
ES13
(+) MFQ
GTPase-associated center (GAC)

Figure 3

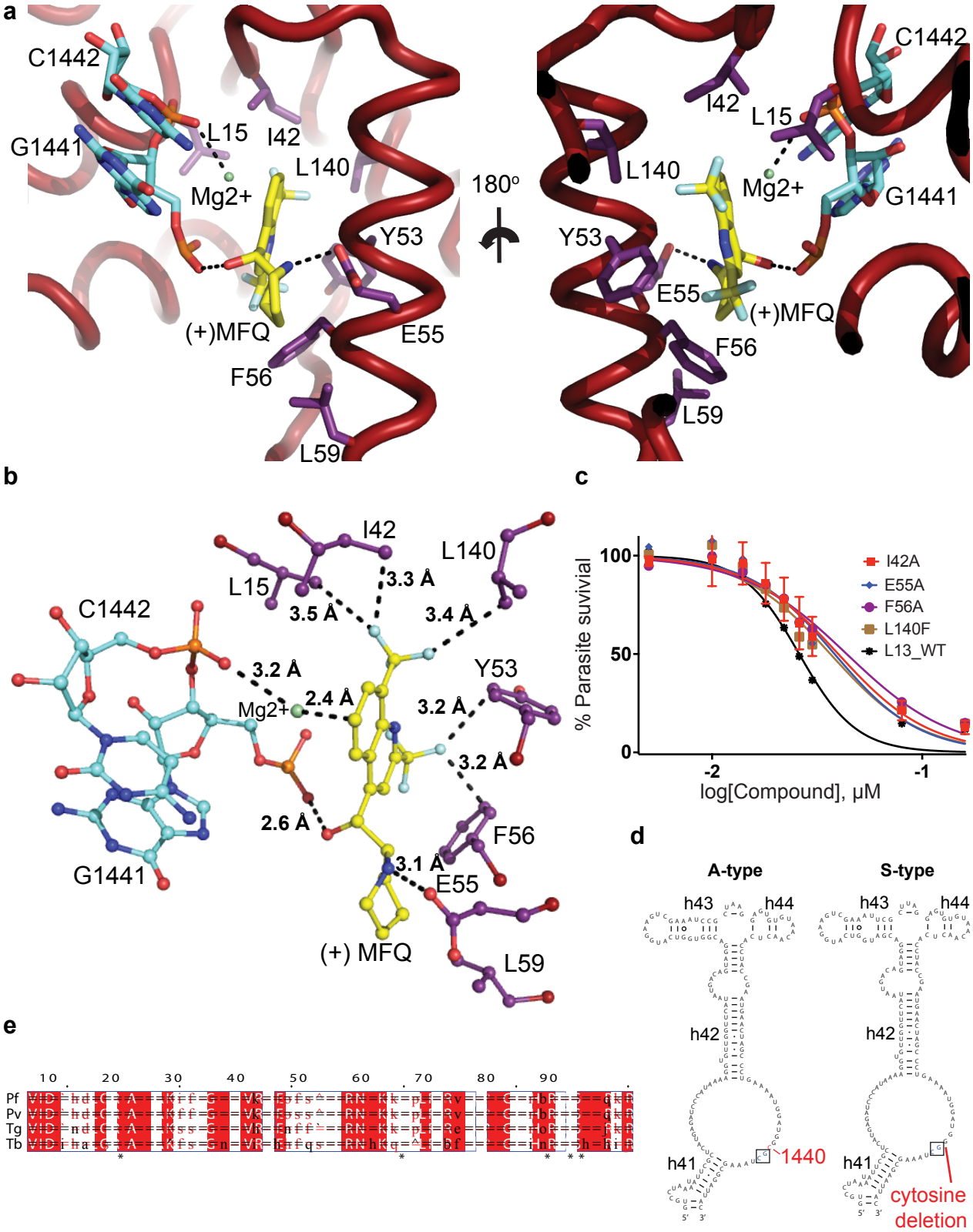
a
C1442
G1441
L15
I42
L140
Mg2+
Y53
(+)MFQ
E55
F56
L59
180°
C1442
I42
L15
L140
Mg2+
G1441
Y53
E55
(+)MFQ
F56
L59
b
I42
L140
L15
3.3 Å
3.5 Å
3.4 Å
C1442
3.2 Å
Y53
Mg2+
2.4 Å
3.2 Å
3.2 Å
2.6 Å
F56
3.1 Å
E55
G1441
(+) MFQ
L59
c
% Parasite suvivial
100
50
0
-2
-1
log[Compound], µM
I42A
E55A
F56A
L140F
L13_WT
d
A-type
S-type
h43
h44
h42
h41
1440
cytosine
deletion
e
10
20
30
40
50
60
70
80
90
Pf
Pv
Tg
Tb

Figure 4

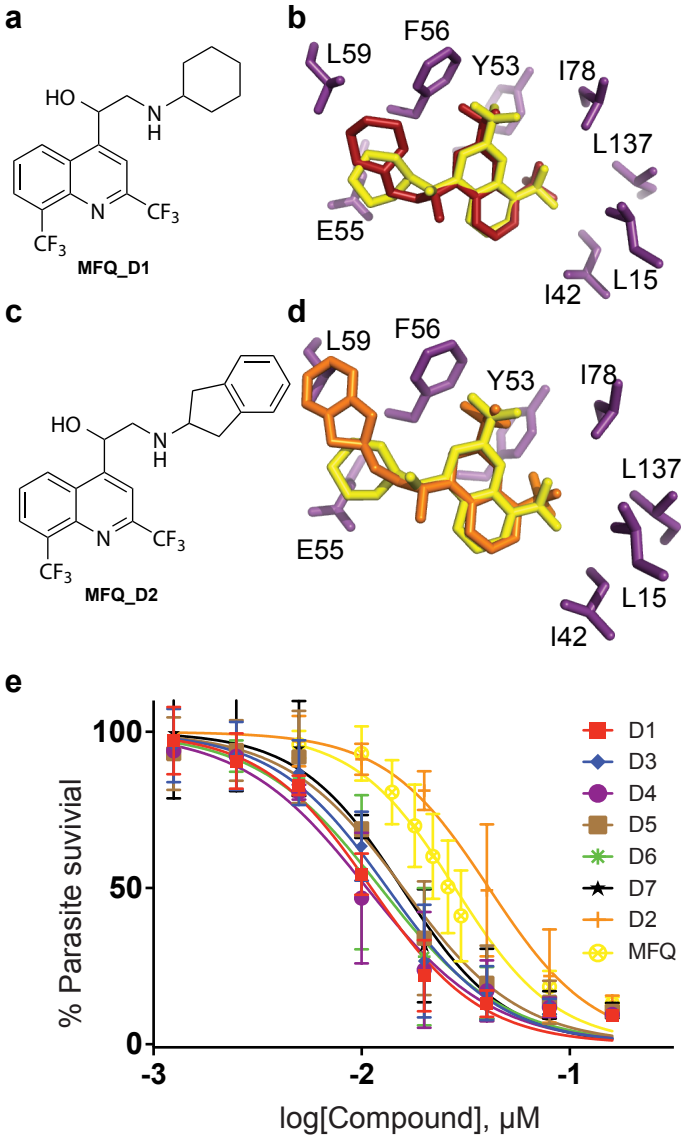
a
HO
N
H
N
CF3
CF3
MFQ_D1
b
L59
F56
Y53
I78
L137
E55
I42
L15
c
HO
N
H
N
CF3
CF3
MFQ_D2
d
L59
F56
Y53
I78
L137
E55
L15
I42
e
100
50
0
-3
-2
-1
% Parasite suvivial
log[Compound], µM
D1
D3
D4
D5
D6
D7
D2
MFQ